Title
Modeling passive scalar dispersion in the atmospheric boundary layer with WRF large-eddy simulation

Journal
Atmospheric Environment, 82

ISSN
13522310

Authors
Nottrott, Anders
Kleissl, Jan
Keeling, Ralph

Publication Date
2014

DOI
10.1016/j.atmosenv.2013.10.026

Peer reviewed

Modeling passive scalar dispersion in the atmospheric boundary layer with WRF large-eddy simulation

Anders Nottrott[1,*], Jan Kleissl[1], Ralph Keeling[2]

[1]University of California, San Diego, Department of Mechanical and Aerospace Engineering
[2]University of California, San Diego, Scripps Institute of Oceanography, Geosciences Research Division

[*]*Corresponding Author*
Anders Nottrott
University of California, San Diego
Department of Mechanical and Aerospace Engineering
9500 Gilman Dr
EBU II - 362
La Jolla, CA 92093-0411
Email: anottrot@ucsd.edu
Tel.: (805) 252-9606

Abstract

The ability of the Weather Research and Forecasting, large-eddy simulation model (WRF-LES) to model passive scalar dispersion from continuous sources located at ground-level and in the surface layer of convective and neutral atmospheric boundary layers was investigated. WRF-LES accurately modeled mean plume trajectories and concentration fields. WRF-LES statistics of concentration fluctuations in the daytime convective boundary layer were similar to data obtained from laboratory experiments and other LES models. However, poor turbulence resolution near the surface in neutral boundary layer simulations caused overestimation of concentration variance in the neutral surface layer. A gradient in the intermittency factor for concentration fluctuations was observed near the surface downwind of ground-level sources in the daytime boundary layer. That observation suggests that the intermittency factor is a promising metric for the estimation of source-sensor distance in practical source determination applications.

Keywords: WRF model; large-eddy simulation; passive scalar; dispersion; atmospheric boundary layer; concentration fluctuations

1. Introduction

1.1 Motivation

The development of a method to quantify greenhouse gas (GHG) emissions from distributed sources using long-term, continuous measurements remains an open problem with important applications for the control, regulation and financial valuation of GHG emissions. California's Global Warming Solutions Act (California AB 32), for example, established a GHG Cap-and-Trade program which includes an enforceable GHG emissions cap and tradable permits to large GHG emitters such as refineries, power plants, and industrial facilities (CARB, 2013). The California Cap-and-Trade Offset Verification Program will rely primarily on a bottom-up framework for regulatory verification of all GHG reductions and removal enhancements. However, the credibility of such a regulatory framework for GHG emissions depends on a reliable method for independent verification and long term monitoring of the actual emissions of market participants. The recent development of a robust and accurate cavity ring-down spectrometer (CRDS; Crosson, 2008) – and the associated field calibration systems (Welp et al, 2012) – has made long-term, continuous field measurements of CO_2 and CH_4 concentrations feasible on national, regional and local spatial scales (Sloop & Novakovskaia, 2013). With the proliferation of CRDSs, and the availability of large volumes of continuous GHG concentration data, a new problem has arisen; namely a lack of capable modeling tools and strategies to interpret the measurements in the context of top-down inventories.

This paper is an assessment of the capability of the Weather Research and Forecasting (WRF) Large-eddy simulation software (hereafter WRF-LES) to model passive scalar dispersion, and thereby GHG dispersion, in the atmospheric boundary layer (ABL). The advantage of WRF-LES over other LES codes is that WRF-LES is integrated within the broader WRF source code which has multi-scale (synoptic to mesoscale) weather simulation capabilities. Two-way nesting of mesoscale and local (LES) scale boundary conditions will be feasible for operational modeling in the near future (Talbot et al, 2012). This capability will facilitate realistic simulations of dispersion from distributed, local scale GHG emissions sources; a process which is significantly impacted by mesoscale forcing. A recent investigation of the influence of different subgrid-scale (SGS) stress models on ABL turbulence simulation in WRF-LES by Kirkil et al (2012) showed that representation of surface layer turbulence at the resolved scale is *especially* poor in WRF-LES, particularly in the neutrally stratified ABL. Poor representation of surface layer turbulence occurred regardless of the chosen SGS model and was attributed to excessive artificial diffusion in the numerical differencing scheme (E. Bou-Zeid, Personal communication, 2012). Thus the goals of this assessment are twofold. The first is to conduct a detailed investigation and validation of passive scalar dispersion in the ABL modeled using WRF-LES. The second is to understand how WRF-LES can be used as a modeling tool to interpret and derive source information from long-term GHG concentration time series measured in the ABL.

The WRF-LES model and setup for numerical experiments are discussed in Section 2. Results of WRF-LES simulations are presented in Section 3. The vertical structure of boundary layer turbulence statistics are discussed in Sections 3.1 and 3.2, mean dispersion trajectories and concentration profiles investigated in Sections 3.3 and 3.4 and concentration fluctuations are investigated in Sections 3.5 and 3.6. A discussion of the results and conclusions are presented in Sections 4 and 5, respectively.

1.2 Literature Review

Pioneering experiments on scalar dispersion in a laboratory scale model of the convective atmospheric boundary layer (CBL) were conducted by Wills & Deardorff (1976, 1981). Data from those experiments established trajectories for plume rise and spread in the CBL downwind of a localized point source of a pollutant. Wills & Deardorff (1976) demonstrated that Taylor's frozen turbulence hypothesis can be applied to transform the dispersion field from a continuous point source (CPS) to that of an instantaneous line source (ILS). That result is important for numerical simulation of ABL dispersion because it can be leveraged to reduce computational cost in turbulent dispersion simulations if the numerical domain is spatially homogeneous in the horizontal directions (see Section 2.3). Later experiments (Deardorff & Willis, 1984) investigated concentration fluctuations downwind of localized scalar sources in the CBL. Large concentration fluctuations occurred and the magnitude of those fluctuations decayed rapidly as a function of downwind distance from the source due to small scale mixing. Shaughnessy & Morton (1977) and Fackrell & Robbins (1982) studied dispersion from CPSs in neutrally stratified boundary layers. Profiles of mean concentration and concentration fluctuations downwind of ground level sources in the neutral ABL maintain a self-similar shape, while dispersion fields from elevated releases preserve downwind self-similarity only in the crosswind direction. Those experiments also showed that, for elevated sources in the neutral boundary layer, the nature of concentration fluctuations downwind of point sources is strongly dependent on the ratio of source size to characteristic length scale of turbulent structures. However, this effect was less apparent for ground level sources. Venkatram and Wyngaard (1988) present an excellent review of parameterizations and experiments on scalar dispersion in the ABL.

ABL dispersion processes span a wide range of length scales, from the integral scale down to the smallest inertial scales and the dissipation range. The large-eddy simulation (LES) technique resolves turbulent structures down to the inertial scales and is well suited to investigate the multi-scale nature of dispersion. Nieuwstadt (1992) studied dispersion from a CPS in a LES of the CBL, and decomposed the dispersion field into two components: a small scale component due to the mixing action of inertial scale eddies and a meandering component caused by large scale motions in the ABL. Nieuwstadt found that meandering was the dominant driver of mean plume spreading near the source, but became small relative to the small scale component as the vertical and crosswind dimensions of the plume approach the integral length scale of the boundary layer. Henn & Sykes (1992) used LES to study concentration fluctuations downwind of a CPS (modeled as volume source at grid resolution) dispersing in a convective boundary layer. Henn & Sykes observed large variability in scalar concentration due to the formation of "concentration filaments" generated by vortical structures in the ABL turbulence field. Yee & Chan (1997) expanded the work of Henn & Sykes and developed a model probability distribution function for concentration fluctuations using a gamma distribution. The LES study of Dosio et al (2003) investigated passive scalar dispersion over a wide range of stability conditions from near neutral to strongly convective and developed new parameterizations for mean dispersion that are valid from neutral through strongly convective conditions.

Nomenclature

c	scalar concentration
c_*	dimensionless scalar concentration
e	Coriolis parameter; vertical component
F	forcing term in the Navier-Stokes equations
f	Coriolis parameter; horizontal component
K_ϕ	scalar eddy diffusivity coefficient
L	Obukhov length
L_x, L_y, L_z	streamwise, crosswind horizontal and vertical dimensions of the numerical domain
M	mean wind speed
M_p	mean wind at the average vertical centerline height of the plume
m_z	meandering component of dispersion
N_x, N_y, N_z	streamwise, crosswind horizontal and vertical number of grid points in the numerical domain
p	pressure
S	continuous source term in the scalar advection-diffusion equation
s_z	spreading component of dispersion
t	time since instantaneous line source release
U_g	geostrophic wind speed
u	along wind (streamwise) component of velocity (u_1)
u_*	friction velocity
v	crosswind horizontal component of velocity (u_2)
w	vertical component of velocity (u_3)
w_*	Deardorff convective velocity scale
w_m	modified velocity scale
X	dimensionless downwind distance
X_m	modified dimensionless downwind distance
x	along wind (streamwise) direction
y	crosswind horizontal direction
z	vertical direction
$\bar{z}$	mean plume vertical centerline height
z_i	inversion height
z_l	local plume vertical centerline height
z_o	aerodynamic roughness
Greek Symbols	
γ	intermittency factor
Δ	numerical grid spacing
θ	potential temperature
ν	kinematic viscosity
ρ	fluid density
σ	plume width
τ	subgrid scale stress tensor
ϕ	scalar mass
Superscript	
'	fluctuation velocity component (as in Reynolds average) or plume width relative to source location
Subscript	
i, j	component indices for vector quantities
p	quantity measured on the plume centerline
s	quantity at the surface
T	threshold value
t	with respect to time
Symbols	
$\sim$	filtered variable
$-$	ensemble or time averaged variable

2. Methodology

2.1 Background

The Weather Research and Forecasting model (WRF; Skamarock & Klemp, 2008) is a community model developed by the National Center for Atmospheric Research (NCAR) and the National Oceanic and Atmospheric Administration (NOAA). WRF has multi-scale, nested simulation capability (from synoptic to local scales), includes real-world land-use and topographic data, and has the capability to ingest regional-scale meteorological forcing data. WRF is designed to run on massively parallel computers, and it is well documented with a broad user base and support group. The Advanced Research WRF (ARW) implements a fully compressible, Euler non-hydrostatic dynamics solver that is conservative for scalar variables. ARW can run in a LES mode (WRF-LES).

Large-eddy simulation provides a framework to obtain turbulence data for ABL wind and scalar fields at greater spatiotemporal resolution than mesoscale atmospheric models or direct measurements. The LES technique directly resolves large turbulent motions in three-dimensions by computing a numerical solution to the filtered Navier-Stokes equations, while the effects of small scale motions are parameterized with a SGS model. The filtered mass conservation and Navier-Stokes equations are (Deardorff, 1970)

$$\partial_i \widetilde{u_i} = 0\,, \tag{1}$$

$$\partial_t \widetilde{u_i} + \partial_j \widetilde{u_i}\widetilde{u_j} = \nu \partial_j \partial_j \widetilde{u_i} - \frac{1}{\rho}\partial_i \tilde{p} - \partial_j \tau_{ij} + \widetilde{F_i}\,, \tag{2}$$

where $\widetilde{u_i}$ is the i^{th} component of filtered velocity field, $\tilde{p}$ is the filtered pressure and τ_{ij} is the subgrid-scale stress tensor. ν and ρ are the fluid kinematic viscosity and density, respectively. $\widetilde{F_i}$ is a general forcing term, e.g. Coriolis force due the earth's rotation. ∂_j represents a spatial derivative while ∂_t is a derivative with respect to time. Einstein's summation notation is used in Eqs. 1 and 2 where $i, j \in [1,2,3]$. Closure of Eq. 2 is obtained by modeling τ_{ij} (for more details of SGS models in WRF-LES see Kirkil et al, 2012). Eqs. 1 and 2 are written for incompressible flow and represent an approximation the full compressible solution that is solved in WRF-LES. The WRF-LES dynamical core uses finite differences (rather than a pseudospectral method) to compute spatial derivatives. Passive scalar dispersion is modeled in WRF-LES by solving the filtered advection-diffusion equation for the atmospheric boundary layer

$$\partial_t \tilde{\phi} + \widetilde{u_j}\partial_j \tilde{\phi} = -\partial_j \widetilde{u_j \phi} + S(x_j), \tag{3}$$

where $\tilde{\phi}$ is the resolved (filtered) scalar mass concentration, $\widetilde{u_j\phi}$ is the SGS scalar mass flux and $S(x_j)$ is the continuous source function. Molecular diffusion is assumed to be negligible in the high Reynolds number limit. The SGS scalar flux is modeled as $\widetilde{u_j\phi} = -K_\phi \partial_j \tilde{\phi}$, where K_ϕ is the SGS scalar eddy diffusivity coefficient.

Nieuwstadt (1992) defined the downwind trajectory of a scalar concentration field in terms of the centroid and first moment of the spatial distribution of the concentration field. The parameters used in this paper to describe the downwind plume trajectory in the *x-z* plane are (see Figure 1): the local (or instantaneous) plume centerline height (z_l), the average plume centerline height ($\bar{z}$), the total vertical dispersion (σ_z), the total vertical dispersion relative to the source height ($\sigma_z{}'$), the spreading component about the local centerline height (s_z) and the meandering component about the average centerline height (m_z). Analogous parameters are also defined for the crosswind trajectory in the *x*-*y* plane. The reader is referred to Nieuwstadt (1992) and Appendix A for mathematical definitions of these variables.

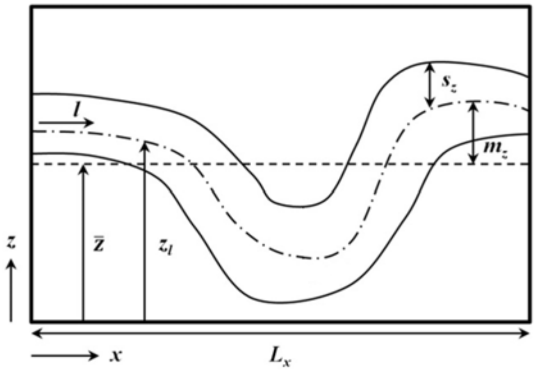

Figure 1 – A schematic of a dispersing ILS illustrating the parameters that describe the downwind trajectory of the scalar field. The *x*-axis is aligned with the mean wind $M = (\bar{u}^2 + \bar{v}^2)^{1/2}$. The parameters shown here are functions in the *x*-*z* plane, and the equivalent parameters in the *x*-*y* plane are analogous. Adapted from Nieuwstadt (1992).

2.2 WRF configuration

Namelist Option	Setting (Value)
Turbulence and mixing (diff_opt)	Mixing in physical space; full diffusion (2)
Eddy coefficient (km_opt)	3D Smagorinsky first order closure (3)
Subgrid-scale model (sfs_opt)	Nonlinear backscatter and anisotropy (0)
Damping layer option (damp_opt)	w-Rayleigh damping (3)
w-Rayleigh damping coefficient (dampcoef)	0.2
Coriolis force (pert_coriolis)	Coriolis only acts on wind departures from geostrophic balance (true)
Lateral boundary conditions (periodic_x, periodic_y)	Periodic lateral boundary conditions (true)
Upper boundary condition (top_lid)	Rigid lid (true)
Surface layer option (sf_sfclay_physics)	Monin-Obukhov scheme (1)
Surface heat and moisture fluxes (isfflx)	Specified surface heat flux (2)
Scalar advection option (scalar_adv_opt)	Positive-definite advection of scalars (1)

Table 1 – Configuration of namelist options for WRF-LES

The WRF-LES 'namelist' configuration used in this study is listed in Table 1. Fifth and third-order finite difference schemes for momentum and scalars were used in the horizontal and vertical directions, respectively. The third order Runge-Kutta scheme was used for time integration. The passive scalar for ABL dispersion simulations was activated by setting the 'tracer_opt' namelist parameter to a value of '2'. A mass source of passive scalar was initialized by modifying the tracer variable loop in 'solve_em.F' subroutine. Periodic lateral boundary conditions were enforced for the velocity, temperature and scalar, and a no penetration/absorption condition was enforced for the scalar at the lower and upper boundaries so that the total scalar mass within the domain was conserved.

2.3 Description of Numerical Experiments

Seven simulation cases were run for a range of ABL stability conditions from neutral through strongly convective, and six different domain configurations were used. The aerodynamic roughness length was set to $z_o = 0.15$ m for all domains and the Coriolis parameters were $f = 8.5 \cdot 10^{-5}$ Hz and $e = 0$ Hz corresponding to an approximate latitude of 36ºN. All simulations were spun up until surface averaged shear stress and domain averaged turbulence kinetic energy were nearly constant in time. Turbulence and boundary layer parameters for all simulations are listed in Table 2. The upper 250 meters of the domain for the CBL cases was allocated as damping layer to prevent the reflection of gravity waves, and the inversion height (z_i) ranged from about 900 m to 1200 m depending on the amount of surface heat flux and time in the simulation. Empirical testing of WRF-LES for the neutral ABL simulations demonstrated that a deep neutral boundary layer could not be maintained because turbulent mixing at the inversion caused warm air from above the inversion to be entrained downward into the boundary layer. This resulted in the formation of a stable temperature profile throughout the boundary layer after a few hours of simulation time (when the boundary layer turbulence was fully developed). Therefore, a damping layer of thickness 250 m was applied at the top of the domain to maintain a deep neutral BL and to simulate dynamic effects of a temperature inversion in the neutral ABL simulation. The domain resolution was varied to investigate the resolution dependence of concentration fluctuations and observed errors in turbulence fields.

Name	L_x, L_y [m]	L_z [m]	$\Delta x, \Delta y$ [m]	Δz [m]	U_g [m s^{-1}]	$\overline{w'\theta'}_s$ [m s^{-1} K^{-1}]	z_i [m]	u_* [m s^{-1}]	w_* [m s^{-1}]	L [m]	$-z_i/L$
B1	7680	1750	30	8	0.5	0.05	1000	0.12	1.19	-2.69	380
B5	7680	1750	30	8	5	0.1	1000	0.28	1.48	-18.6	59
B5HR	3040	1500	10	2.75	5	0.1	900	0.29	1.48	-19.2	52
SB2	7680	1750	30	8	10	0.1	1000	0.49	1.48	-109	11
SB2HR	3040	1500	10	2.75	10	0.1	900	0.50	1.48	-100	10
N	8640	1067	30	8	15	0	815	0.6	0	$-\infty$	0
NHR	7680	1067	15	4	15	0	815	0.6	0	$-\infty$	0

Table 2 – Domain and boundary layer parameters for different numerical experiments in this study. Δz values are approximate because WRF uses vertical pressure coordinates. The simulation names are similar to those in Dosio et al (2003). The inversion heights listed in this table were the initial values at the start of each simulation.

Continuous point sources of a passive scalar were modeled as instantaneous line sources aligned parallel to the streamwise direction under the assumption of Taylor's hypothesis. This approach reduces the computational cost of dispersion simulations (for domains that are spatially homogeneous in the horizontal directions) because dispersion at long downwind distances can be modeled with a relatively small numerical domain by increasing the run time of the simulation instead of the spatial extent of the domain. Ensemble average statistics of scalar concentration at any downwind location can be computed from instantaneous spatial transects of scalar concentration in the domain taken at the appropriate moment in time. The transformation from CPS to ILS is also compatible with periodic boundary conditions because it eliminates the need for sponge boundary conditions for the scalar on the lateral domain boundaries. Different source heights (z_s) were used for passive scalar releases to facilitate comparison of data from the present LES study with data from previous laboratory and numerical experiments. Source heights z_s = 0.0033z_i, 0.07 z_i, 0.19 z_i were used in simulations B3 and B5, z_s = 0.0033 z_i, 0.07 z_i in simulation SB2 and z_s = 0.0043 z_i, 0.07 z_i in simulation N. z_s = 0.0025 z_i, 0.07 z_i in simulation NHR and z_s = 0.0033z_i in simulations B5HR and SB2HR. Sources in domains B3, B5, SB2 and N were represented using 1 grid cell in the crosswind horizontal direction and 2 grid cells in the vertical direction (after Henn & Sykes, 1992 and Dosio et al 2003). Sources in domains B5HR and SB2HR were represented with 3 grid cells in the crosswind horizontal direction and 6 grid cells in the vertical direction, while in domain NHR the source occupied 2 grid cells in the crosswind horizontal direction and 4 grid cells in the vertical direction The initial source volume and scalar mass were constant in all simulations, but sources were represented by more grid points in the higher resolution domains.

3. Results

3.1 Variance profiles

Figures 2 and 3 show normalized vertical profiles of the Reynolds stresses, temperature variance, kinematic heat flux for CBL and neutral ABL (cases B3, N and NHR) compared with data from established LES codes, laboratory experiments and aircraft data. Good agreement was observed between WRF-LES and validation data for the CBL (Figure 2). The peak in the vertical velocity variance occurred around $0.4z_i$ and the vertical profile of kinematic heat flux was linear over the depth of the boundary layer. Agreement between WRF-LES and validation data was also reasonable for the neutral ABL simulations (Figure 3). The magnitude of the maximum streamwise velocity variance in WRF-LES is larger than the other data, however, Moeng et al (2007) (using a less realistic SGS model) observed streamwise velocity variances as large as $9u_*^2$ in WRF-LES. The peak in the vertical velocity variance occurred above the surface layer at a height of $0.2z_i$ in the low resolution domain (case N), but occurred closer to the surface around $0.1z_i$ in the high resolution domain (case NHR). This observation is consistent with the results of Kirkil et al (2012), and indicates that the SGS model is under-dissipative resulting in large $\partial\bar{u}/\partial z$. Bou-Zeid et al. (2005) demonstrated that the Lagrangian scale-dependent dynamic SGS model produces a streamwise velocity and variance profile consistent with similarity theory and observations; however this model is not available in the public release of WRF-LES. The variance profiles in Figure 3 are all within the range of the LES code inter-comparison presented in Andren et al (1994).

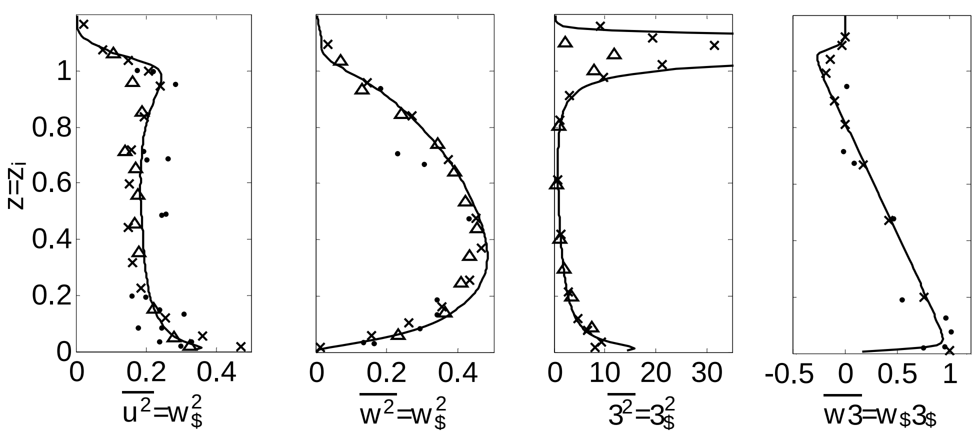

Figure 2 – Vertical profiles of resolved velocity variance, temperature variance and temperature flux normalized by the convective velocity scale and/or convective temperature scale for the CBL (WRF-LES case B3). WRF-LES resolved scales (solid line); LES of Raasch & Etling (1991; crosses); water channel data of Willis & Deardorff (1976; triangles); aircraft data of Lenschow et al (1980; dots).

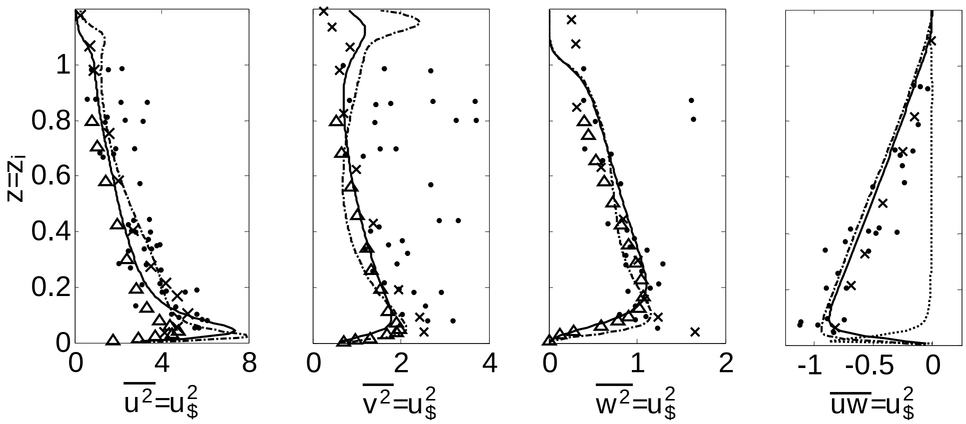

Figure 3 – Vertical profiles of velocity variance and momentum flux normalized by the surface shear stress in the neutral ABL (WRF-LES case N). WRF-LES simulation N resolved scales (solid line) and subgrid-scales (dotted line); WRF-LES simulation NHR resolved scales (dash-dotted line); LES of Moeng & Sullivan (1994; crosses); WRF-LES with nonlinear backscatter and anisotropy SGS model Kirkil et al (2012; triangles) with $\Delta x = \Delta y = 32$ m and $\Delta z = 8$ m; aircraft data from Grant (1986; dots).

3.2 Validity of CPS to ILS transformation

Continuous point source releases of passive scalars were modeled as instantaneous line sources under the assumption of Taylor's hypothesis (Willis & Deardorff, 1976). The transformation between downwind distance and time is $x = M_p t$, where M_p is the mean wind speed at the average vertical centerline height of the plume $\bar{z}$. This transformation is only valid when the intensity of turbulent velocity fluctuations is small compared to the mean wind speed, i.e. $\bar{u_\iota}^2/M_p^2 \ll 1$. Figure 4 shows vertical profiles of velocity variances divided by mean wind speed for all simulations. The assumption of Taylor's hypothesis is not valid for case B3 but is reasonable for the other cases. Dosio et al (2003) found that, although the CPS to ILS transformation was not strictly valid for their B3 case, the mean downwind trajectory of the dispersion field matched experimental data quite well. Nevertheless, Figure 4 indicates that concentration fluctuations from the ILS dispersion field in the B3 boundary layer may not be directly comparable to concentration fluctuations from a CPS released in the same turbulence field, so data from the B3 case was not used to investigate scalar concentration fluctuations.

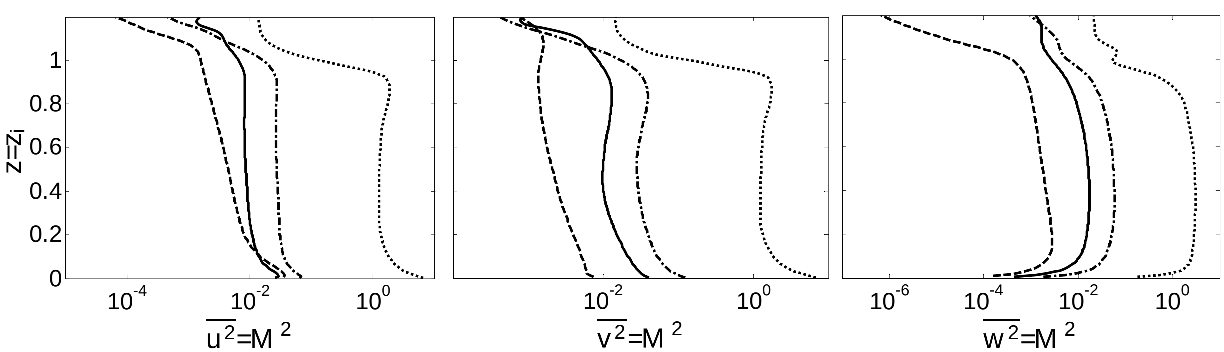

Figure 4 – Vertical profiles of velocity variance to mean wind speed ratio for all simulation cases. B3 (short dash line), B5 (dash-dot line), SB2 (solid line) and N (long dash line). Data for case NHR are not shown because they are similar to those for case N.

3.3 Plume trajectories

A dimensionless downwind distance parameter

$$X = \frac{w_*}{z_i}\frac{x}{M_p} = \frac{w_*}{z_i}t, \tag{4}$$

is defined after Willis & Deardorff (1976), where x is the downwind distance from the source and t is the downwind travel time (consistent with the transformation described in Section 3.2). A modified dimensionless downwind distance X_m is defined by substituting the convective velocity scale in Eq. 3 with a mixed velocity scale w_m. w_m applies when the buoyant and shear turbulent production are of similar magnitude. Moeng & Sullivan (1994) proposed the relationship $w_m^3 = w_*^3 + 5u_*^3$. Figure 5 shows the components of mean dispersion parameters (see Figure 1) modeled with WRF-LES for a surface layer release in the CBL compared with data from laboratory experiments. The modeled mean dispersion parameters generally fall within the range of the experimental data, with the exception of the total horizontal crosswind dispersion (Figure 5c) which becomes smaller than the experimental data for $X > 1.25$. This behavior was also observed in the LES study of Dosio et al (2003). It is interesting that the contribution of the meandering component (m_y) to σ_y becomes relatively constant downwind of $X > 1.25$ although σ_y continues to grow. This observation indicates that beyond $X > 1.25$ the horizontal crosswind dispersion is primarily driven by the spreading component of dispersion (s_z).

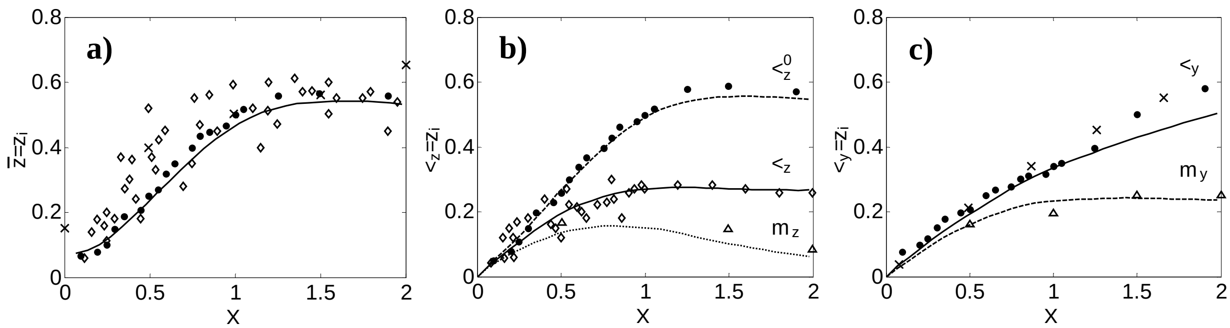

Figure 5 – Validation of mean dispersion parameters for a passive scalar release in the CBL (case B3) plotted as a function of dimensionless downwind distance X (Eq. 4). The source was located at X = 0 and $z_s = 0.07z_i$. **a)** Mean plume height, **b)** total vertical dispersion and vertical meandering component, and **c)** total horizontal crosswind dispersion and crosswind meandering component. WRF-LES results are plotted as continuous lines and experimental data are plotted as symbols; Willis & Deardorff (1976; dots), Briggs (1993; diamonds) and Weil et al (2002; crosses and triangles). Each line in Figure 5b,c shows a different component of dispersion, and the label above each line indicates the variable that corresponds to the appropriate component of dispersion (refer to Section 2.1, Figure 1 and Appendix A for descriptions of these variables).

Figure 6 shows mean dispersion trajectories downwind of point sources in moderately convective (case SB2) and neutral (case N) atmospheric boundary layers, compared with results from the LES of Dosio et al (2003). The mean plume height (Figure 6a) and total vertical dispersion (Figure 6b) are in close agreement with Dosio et al for both the SB2 and N boundary layers. The total horizontal crosswind dispersion (σ_y/z_i; Figure 6c) for the WRF-LES SB2 case is similar to the Dosio et al data for $X_m < 1.25$, but begins to diverge farther downwind. However, σ_y/z_i in the WRF-LES simulation N is significantly smaller than the Dosio et al data. We investigated the dependence of $\sigma_y(X)$ on SGS scalar flux by setting the $-\partial_j \widetilde{u_j \phi}$ term in Eq. 3 to zero. Excluding the $-\partial_j \widetilde{u_j \phi}$ term caused a 5% decrease in $\sigma_y(X)$ at $X = 2.5$. $\sigma_y(X)$ was about 10% larger at $X = 2.5$ for the surface layer release ($z_s = 0.07z_i$) in the N case when compared with the NHR case. This result suggests a systematic model bias for $K_{\phi,h}$ (see Section 4).

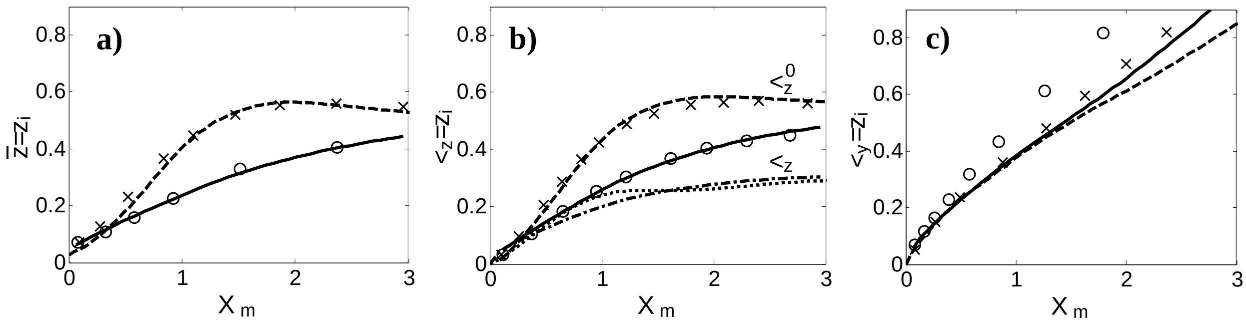

Figure 6 – Validation of mean dispersion parameters for a passive scalar release in moderately convective (case SB2) and neutral atmospheric boundary layers (case N) plotted as a function of dimensionless downwind distance X_m (Eq. 4). The source was located at $X_m = 0$ and $z_s = 0.07z_i$. **a)** Mean plume height, **b)** total vertical dispersion, and **c)** total horizontal crosswind dispersion. WRF-LES results are plotted with continuous lines (SB2 long and short dash lines; N solid and dash-dot lines). WRF-LES dispersion fields are compared with LES data from Dosio et al (2003) plotted with crosses for SB2 and circles for N. Each pair of lines in Figure 6b (long dash/solid and short dash/dash-dot) shows a different component of dispersion. The label above indicates the variable that corresponds to the appropriate component of dispersion (refer to Section 2.1, Figure 1 and Appendix A for descriptions of these variables).

3.4 Mean concentration profiles

Figure 7 shows contours of dimensionless mean concentration $c_* = \bar{c}(x,y,z)z_i^2M_p/S$ for a surface layer source in the B3 simulation. Figure 7a is a vertical cross-section along the plume centerline, while Figure 7b shows total c_* from the surface to the inversion height. The magnitude and shape of c_* contours are very similar to the laboratory measurements of Willis & Deardorff (1976), although the plume width (Figure 7b) is slightly underestimated by WRF-LES for $X > 1.25$ (consistent with Figure 5c). Profiles of average scalar concentration in the CBL do not exhibit self-similar behavior when normalized σ_y or σ_z, because CBL turbulence is dominated by large coherent structures and therefore non-Gaussian (for example refer to the laboratory data presented in Willis & Deardorff, 1976).

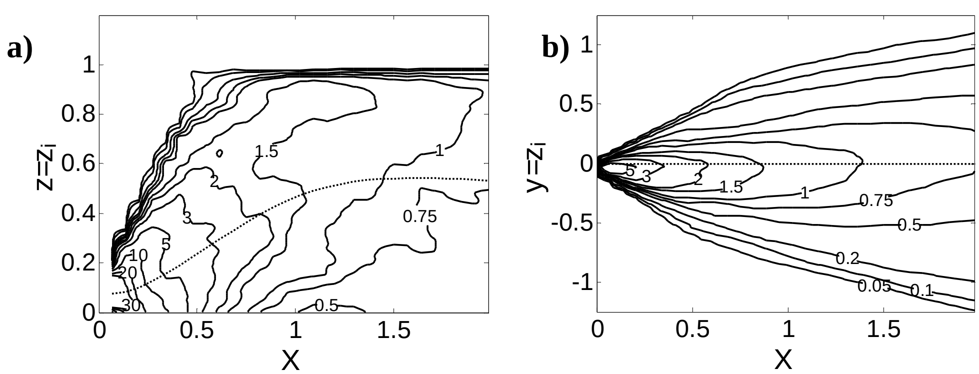

Figure 7 – Contours of dimensionless mean concentration $c_* = \bar{c}(x,y,z)z_i^2M_p/S$ for a surface layer ($z_s = 0.07z_i$) release in the B3 simulation. **a)** Vertical cross-section along the plume centerline; **b)** integrated over the z-direction from the surface to the inversion height. The dashed lines indicate the plume centerline ($\bar{z}$ and $\bar{y}$).

Figure 8 shows vertical profiles of mean concentration along the plume centerline at different locations downwind of sources released at ground-level and in the surface layer for simulation case N. Figure 8a shows the expected self-similarity of the mean concentration field due to the presence of the ground. Consistent with the water channel experiments of Fackrell & Robins (1982) self-similarity does not occur in the vertical direction for surface layer releases (Figure

8b). Figure 9 confirms self-similarity of the crosswind horizontal concentration profiles in the neutral boundary layer simulation (Shaughnessy & Morton, 1977). The slight negative skewness apparent in Figure 9 occurred because the mean wind direction was not exactly parallel to the direction of the ILS when the source was initialized due to the Coriolis force. Although the data shown in Figure 9 are for a surface layer source, self-similarity was also observed for the ground level source.

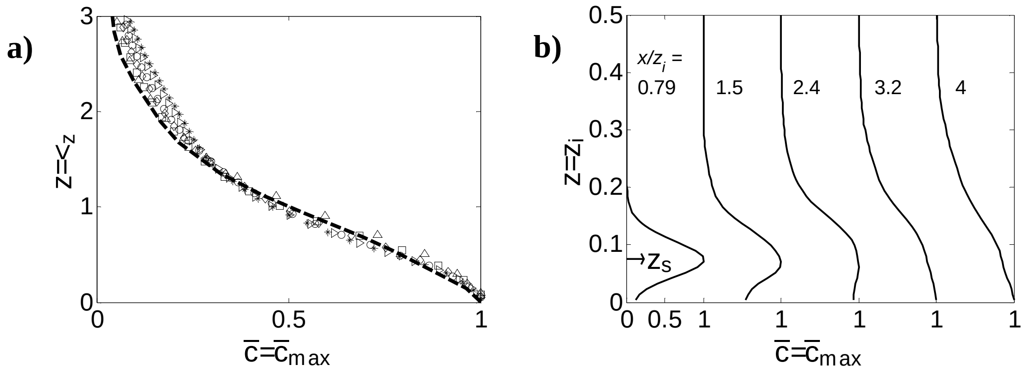

Figure 8 – Vertical profiles of mean concentration at various downwind locations along the plume centerline for **a)** a ground-level source ($z_s = 0.0043z_i$), and **b)** a source in the surface layer ($z_s = 0.07z_i$) in the N simulation. The mean concentration is normalized by the maximum mean concentration at each downwind location. Figure 8a: $x/z_i = 2.1$ (triangles); 3.0 (squares); 3.9 (diamonds); 4.7 (circles); 5.6 (leftward arrows); 6.5 (stars). Data from Fackrell & Robbins (1982) are shown as the dashed line in Figure 12a. Profiles in Figure 8b are offset by $\bar{c}/\bar{c}_{max} = 1$ for readability.

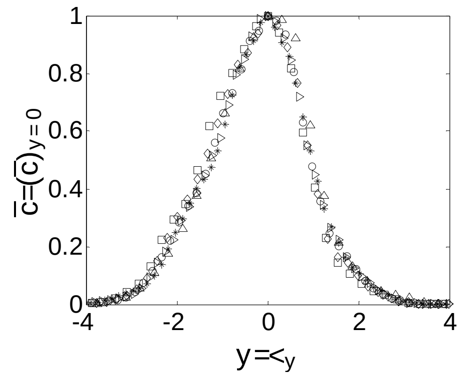

Figure 9 – Self-similarity of horizontal crosswind profiles of mean concentration at various downwind locations at the height of the plume vertical centerline ($\bar{z}$) for a surface layer ($z_s = 0.07z_i$) source in case N. The mean concentration is normalized by the maximum mean concentration (i.e. mean concentration at $y = 0$) at each downwind location. $x/z_i = 2.4$ (triangles); 3.2 (squares); 4.0 (diamonds); 4.9 (circles); 5.8 (leftward arrows); 6.6 (stars).

3.5 Concentration fluctuations

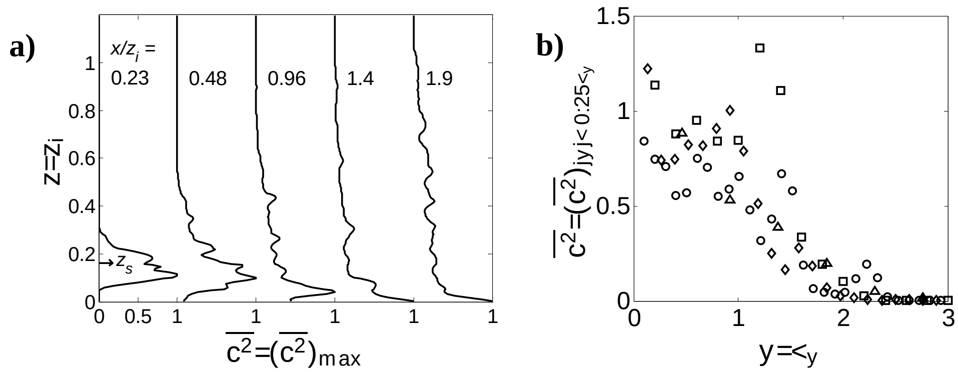

Figure 10 - Vertical and horizontal profiles of normalized concentration variance at different distances downwind of an elevated release located at $z_s = 0.19z_i$ in the B5 simulation. **a)** Vertical profiles of concentration variance normalized by the maximum variance at each downwind position. **b)** Crosswind horizontal profiles of concentration variance at the vertical centerline height normalized by the mean variance in the region $|y| < 0.25\sigma_y$. $x/z_i = 0.23$ (triangles); 0.70 (squares); 1.2 (diamonds); 1.6 (circles). Profiles in Figure 10a are offset by $\overline{c^2}/(\overline{c^2})_{max} = 1$ for readability.

Available data on concentration fluctuations in the CBL are somewhat unstructured making direct validation of the present LES experiments challenging. Figure 10 shows vertical and horizontal profiles of normalized concentration variance at different distances downwind of an elevated release located at $z_s = 0.19z_i$ in the B5 simulation. The variance profiles in Figure 10a illustrate downward motion of the plume (i.e. looping) downwind of the source which is a characteristic feature of neutrally buoyant releases from elevated sources in the CBL (Henn & Sykes, 1992). Figure 10b shows crosswind horizontal profiles of concentration variance, normalized by the mean variance in the region $|y| < 0.25\sigma_y$, at the centerline height of the plume. The WRF-LES model correctly captures the peak in the concentration variance that occurs in the range $0.5 < y/\sigma_y < 1.5$ although there is considerable scatter in the LES data (Venkatram & Wyngaard, 1988). Figure 11 shows a comparison of ground-level concentration fluctuation standard deviation from the same elevated release as in Figure 10 with data from Henn & Sykes (1992). The data do not match exactly because the sources were located at slightly different heights in the boundary layer, however, the magnitudes of the data are similar. The larger standard deviation of the WRF-LES data may also be due to the higher spatial resolution used in our simulations compared to Henn & Sykes.

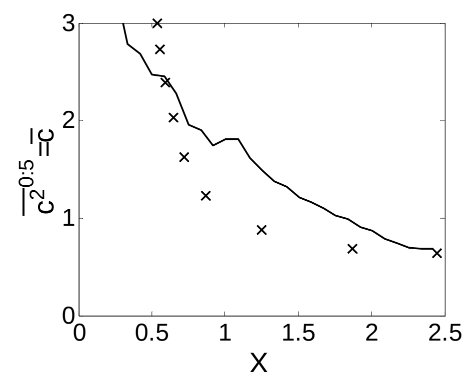

Figure 11 – Standard deviation of ground-level concentration fluctuations downwind of an elevated source normalized by the mean ground level concentration. The solid line shows WRF-LES data for a source located at $z_s =$

$0.19z_i$ in the B5 simulation. The crosses are LES data from Henn & Sykes (1992) who modeled an elevated source at $z_s = 0.25z_i$ with LES.

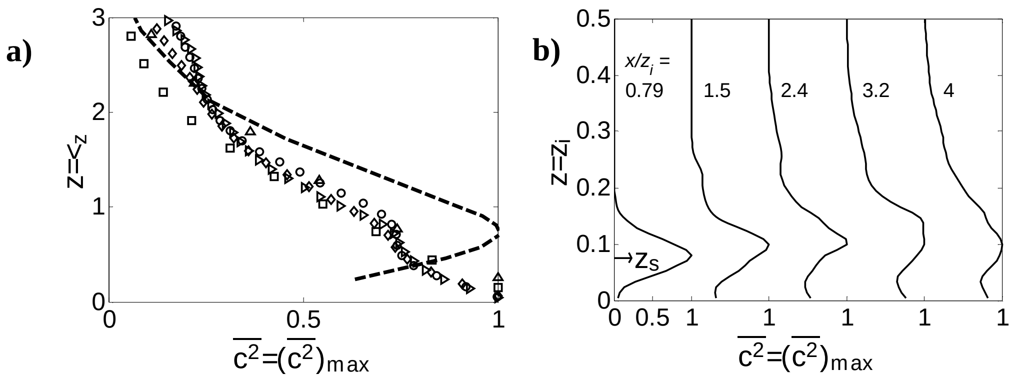

Figure 12 - Vertical profiles of concentration variance at different downwind locations along the plume centerline for **a)** a ground-level source ($z_s = 0.0043z_i$), and **b)** a source in the surface layer ($z_s = 0.07z_i$) in the N simulation. The concentration variance in normalized by the maximum variance at each downwind location. Figure 12a: $x/z_i = 0.59$ (triangles); 1.3 (squares); 3.9 (diamonds); 4.7 (circles); 5.6 (arrows). Data from Fackrell & Robbins (1982) are shown as the dashed line in Figure 12a. Profiles in Figure 12b are offset by $\bar{c}/\bar{c}_{max} = 1$ for readability.

Figure 12 shows vertical profiles of normalized concentration variance for ground-level and surface layer sources in the neutrally stratified boundary layer (simulation N). The wind tunnel experiments of Fackrell & Robbins (1982) showed that vertical profiles of normalized variance for ground-level sources are self-similar along the plume centerline axis with a maximum value at $z/\sigma_z \approx 0.75$. Fackrell & Robbins also hypothesized that the value of $\overline{c^2}$ should tend toward zero at the surface although their lowest measurements did not extend below $0.05z_i$. The WRF-LES data in Figure 12a are approximately self-similar. However, although there is a local maximum in the vertical profiles at $z/\sigma_z \approx 0.75$, the normalized variance approaches a value of 1 at the surface rather than 0. The vertical profiles for the surface layer source (Figure 12b) exhibit the correct upward trend for $\left(\overline{c^2}\right)_{max}$, but also show a local maximum in concentration variance at the surface. Figure 13 shows crosswind horizontal profiles of normalized concentration variance at different distances downwind at the height of plume vertical centerline for the surface layer release ($z_s = 0.07z_i$). The data in Figure 13 exhibit the weak peak in concentration variance that occurs at $y/\sigma_y \approx 0.5$ consistent with wind tunnel data (see Figure 7 in Fackrell & Robbins; 1982). The data in Figure 13 are not expected to preserve self-similarity.

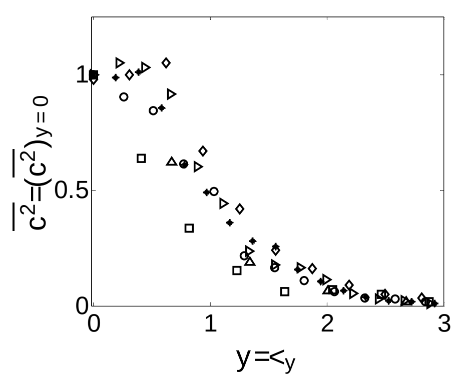

Figure 13 – Crosswind horizontal profiles of concentration variance at the height of the plume vertical centerline, normalized by the variance at the horizontal centerline of the plume (i.e. the variance at $y = 0$) for a surface layer

release $z_s = 0.07z_i$. $x/z_i = 0.79$ (triangles); 1.5 (squares); 2.4 (diamonds); 3.2 (circles); 4.0 (leftward arrows); 4.9 (stars).

3.6 Intermittency factor for ground-level sources

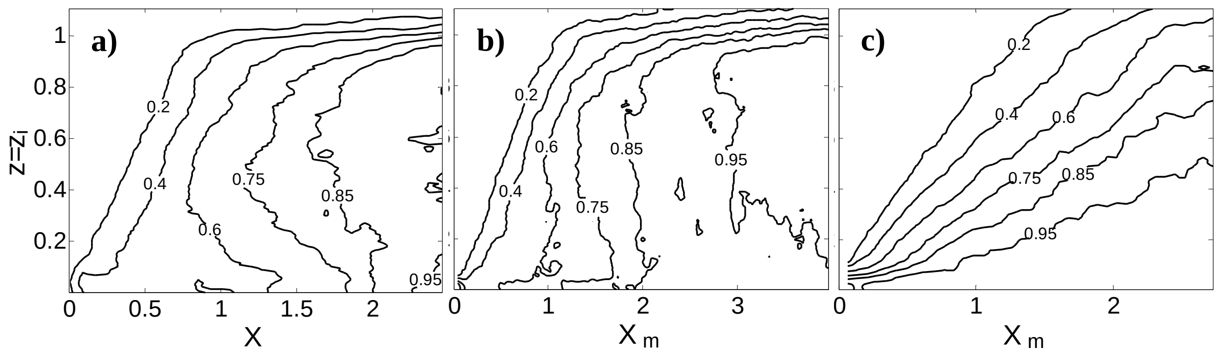

Figure 14 - Contours of the intermittency factor (γ) in the *x-z* plane along the horizontal centerline of the plume for ground-level releases located at $X = 0$. **a)** simulation B5 ($z_s = 0.0033z_i$); **b)** simulation SB2 ($z_s = 0.0033z_i$); **c)** simulation N ($z_s = 0.0043z_i$). The threshold was $c_T = 0.1\bar{c}$.

The intermittency factor (γ) for a timeseries of an arbitrary scalar (c) is defined as the fraction of time during which the magnitude of c exceeds some threshold value (c_T): $\gamma \equiv \tau/T$, T is the total length of the timeseries and τ is the total length of time during which $c > c_T$. The intermittency factor is an alternative metric to standard statistical moments for quantifying concentration variability in timeseries of measurements. Figure 14 shows contours of γ in the *x-z* plane along the horizontal centerline of the plume for ground-level releases in simulations B5, SB2 and N. Direct comparison of γ with data from experiments or other LES studies is difficult because γ depends on both source area relative to the characteristic length scale of turbulence (Fackrell & Robbins, 1982) and the velocity of the source gas (Venkatram & Wyngaard, 1988). Nevertheless the magnitude and shape of contours downwind of the source in Figure 14a are comparable to convection tank data from the experiments of Willis & Deardorff (presented in Venkatram & Wyngaard, 1988). The intermittency factor profile for the B5HR simulation was nearly identical to Figure 14a, although the profile for SB2HR showed a weaker downwind gradient in the intermittency factor near the surface than observed in SB2 (Figure 14b). A value of $\gamma \geq 0.95$ downwind of a ground-level source in the neutral boundary layer (Figure 14c) is also consistent with the wind tunnel data of Fackrell & Robbins (1982). The most interesting feature of Figure 14 is the gradient in γ that occurs near the surface downwind of sources in the convective boundary layer (Figures 14a,b). That gradient may provide the ability to estimate the source-sensor distance for sources upwind of an in situ concentration measurement in the daytime atmospheric surface layer.

4. Discussion

WRF-LES is a useful and relatively accessible tool for simulating turbulence and passive scalar dispersion in the atmospheric boundary layer. There are some real practical advantages of WRF-LES when compared with other LES codes including, the regular/modular structure of the source code, extensive documentation and example simulations, widely connected user base and helpful support group. The most significant disadvantage of WRF-LES appears to be excessive numerical diffusion in the dynamic solver which causes poor resolution of surface layer turbulence in shear driven boundary layers (Kirkil et al, 2012). We have shown that this problem can be mitigated by increasing the spatial resolution of the numerical grid (Figure 3), but the computational cost of that solution is usually prohibitive.

WRF-LES accurately modeled mean dispersion parameters for passive scalars in the CBL. However, as the relative contribution of shear production to buoyant production increased (i.e. $L \rightarrow -\infty$) WRF-LES tended to underestimate the growth of the crosswind horizontal plume width as a function of downwind distance. This error was especially significant in the purely shear driven (neutral) turbulent boundary layer (Figure 6c). The underestimation of σ_y/z_i in the WRF-LES simulation N was caused by a bias in the horizontal eddy diffusivity coefficient for scalars ($K_{\phi,h}$) because WRF-LES assumes $K_{\phi,h} = 3K_{m,h}$, where $K_{m,h}$ is the horizontal eddy diffusivity for momentum and $K_{m,h}$ is calculated by the SGS model for the momentum equation (Eq. 2). This is claim is supported by the fact that a 10% increase in σ_y/z_i was observed when a source of identical volume was modeled in case NHR instead of case N. It is unlikely that the underestimation of $\sigma_y(X)$ was related to poor resolution of the source because the bias increases with downwind distance where the plume is resolved by O(10) grid cells. The observed bias in in the scalar field is also consistent with the under estimation of the streamwise and crosswind horizontal turbulent velocity variances in Figure 4. Future WRF-LES research should focus on improving parameterizations for the eddy diffusivity coefficients in the wall-layer where a zonal approach like the Two-Layer Model (TLM; Piomeli & Balaras, 2002) may be more appropriate for common grid spacing of O(10 m).

That self-similarity was preserved in the mean concentration profiles downwind of the ground-level source in the neutral simulations (Figures 8a and 9) indicates that *relative* plume dispersion was modeled correctly. As an aside, replacing w_m by u_* results in better agreement between the neutral boundary layer data in Figure 6c (not shown; w_m = 1.0 m s^{-1} see Eq. 4, u_* = 0.6 m s^{-1} for the N and NHR cases), however, a direct comparison to Dosio et al (2003) is not possible because they did not provide values of the friction and convective velocities. Therefore, there is an issue with this commonly used velocity scale for forced convection not being an appropriate velocity scale for normalizing the downwind distance variable in neutral and near-neutral boundary layers

One disadvantage of LES for dispersion simulations is that the minimum source size is limited by the spatial resolution of the numerical grid. Due to the high computational cost of LES, the smallest source volume that can be practically represented in full scale simulations of the ABL is around 1000 m^3. The effect of this limitation on concentration timeseries modeled with LES is a low pass filtering of the true signal. Weil et al (2012) addressed this issue by incorporating a stochastic, Lagrangian particle dispersion model into an LES of the CBL. Validation of scalar concentration fluctuations modeled with WRF-LES was also complicated by the fact that measures of concentration variability depend on source size, effluent velocity and grid resolution; all of which vary considerably among data presented in existing literature. Reasonable agreement was observed between concentration variance profiles calculated from the LES data of Henn & Sykes (1992) and data from the present study in the CBL (Figures 10 and 11). However, for case N WRF-LES greatly overestimates the magnitude of the concentration variance in the neutral surface layer compared to wind tunnel experiments (Figure 12a). This issue is likely related to poor turbulence resolution in the neutral surface layer, because smaller $\overline{u}_i$ causes less dispersion of concentration filaments which results in large concentration fluctuations near the surface and thereby increased concentration variance. Timeseries of scalar concentration in the atmospheric boundary layer are non-stationary and non-Gaussian. Therefore the intermittency factor (γ) is a useful alternative metric to mean and variance for quantifying concentration variability, because the relationship between the low order moments of a timeseries of concentration measurements and the probability distribution for the instantaneous concentration magnitude is not straightforward (Yee & Chan, 1997).

5. Conclusion

WRF-LES accurately modeled mean plume trajectories and concentration fields of passive scalar dispersion from continuous point sources. WRF-LES modeled statistics of concentration fluctuations in the convective boundary layer and the neutral boundary layer showed reasonable agreement with laboratory experiments and other LES. However, poor turbulence resolution near the surface in neutral atmospheric boundary layer simulations caused overestimation of concentration variance in the neutral surface layer. A gradient in the intermittency factor (γ) was observed near the surface downwind of ground-level sources in the daytime convective boundary layer. This finding indicates that γ is a promising metric for the estimation of source-sensor distance in practical, local-scale source determination applications where the location of upwind sources within the concentration footprint of a measurement sensor is unknown. However, the relationship between γ and source-sensor range may depend on mesoscale forcing, topography and/or source area effects which would have to be quantified with site specific models.

Acknowledgements

The authors gratefully acknowledge Jeff Mirocha, Alessandro Dosio, the staff at the NCAR WRF helpdesk, and the anonymous reviewers who provided helpful comments and suggestions on the first draft of this manuscript. Thanks to Anirban Garai for many helpful discussions on atmospheric boundary layer turbulence and numerical simulation of turbulent flows.

Appendix A

Mathematical definitions of the variables that define the trajectory of a scalar concentration field downwind of the source (refer to Section 2.1 and Figure 1). Eqs. A1-A6 are reproduced from Nieuwstadt (1992).

$$z_l = \frac{\iint_{A(x)} cz\, dy\, dz}{\iint_{A(x)} c\, dy\, dz}, \tag{A1}$$

$$\bar{z} = \frac{\int_V cz\, dx\, dy\, dz}{\int_V c\, dx\, dy\, dz}, \tag{A2}$$

$$s_z{}^2 = \frac{\int_V c(z - z_l)^2\, dx\, dy\, dz}{\int_V c\, dx\, dy\, dz}, \tag{A3}$$

$$m_z{}^2 = \frac{\int_V c(z_l - \bar{z})^2\, dx\, dy\, dz}{\int_V c\, dx\, dy\, dz}, \tag{A4}$$

$$\sigma_z^2 = s_z{}^2 + m_z{}^2 \tag{A5}$$

$$\sigma_z{}'^2 = \frac{\int_V c(z - z_s)^2\, dx\, dy\, dz}{\int_V c\, dx\, dy\, dz} \tag{A6}$$

z_l is the local (or instantaneous) plume centerline height, $\bar{z}$ is the average plume centerline height, s_z is the spreading component about the local centerline height and m_z is the meandering component about the average centerline height, σ_z is the total vertical dispersion, $\sigma_z{}'$ is the total vertical dispersion relative to the source height. *A(x)* in Eq. A1 refers to the cross-sectional area of the numerical domain in *y-z* plane, *V* in Eqs. A2-A6 is the total volume of the numerical domain and z_s is the source height. The same variables may also be used to define the crosswind horizontal trajectory of the plume. Note that $\sigma_y^2 = \sigma_y{}'^2$, because $y_s = 0$ by definition.

References

1. Andren A., Brown A.R., Graf J., Mason P.J., Moeng C-H., Nieuwstadt F.T.M., Schumann U., 1994, Large-eddy simulation of a neutrally stratified boundary layer: A comparison of four computer codes, *Quarterly Journal of the Royal Meteorological Society* 120, pp. 1457-1484.

2. Bou-Zeid E., Meneveau C., Parlange M., 2005, A scale-dependent Lagrangian dynamic model for large eddy simulation of complex turbulent flows, *Physics of Fluids* 17, pp. 025105.

3. California Environmental Protection Agency, Air Resources Board (CARB), "Cap-and-Trade Program", Available online at <http://www.arb.ca.gov/cc/capandtrade/capandtrade.htm>, Accessed March 18th, 2013.

4. Crosson E.R., 2008, A cavity ring-down analyzer for measuring atmospheric levels of methane, carbon dioxide, and water vapor, *Applied Physics B: Lasers and Optics* 92**(3)**, pp. 403-408.

5. Deardorff J.W., 1970, A numerical study of three-dimensional turbulent channel flow at large Reynolds numbers, *Journal of Fluid Mechanics* 40**(2)**, pp. 453-480.

6. Deardorff J.W., Willis G.E., 1984, Groundlevel concentration fluctuations from a buoyant and a non-buoyant source within a laboratory convectively mixed layer, *Atmospheric Environment* 18**(7)**, 1297-1309.

7. Dosio A., Arellano J.V-G., Holtslag A.A.M., Builtjes P.J.H., 2003, Dispersion of a passive tracer in buoyancy- and shear-driven boundary layers, *Journal of Applied Meteorology* 42, pp. 1116-1130.

8. Fackrell J.E., Robins A.G., 1982, Concentration fluctuations and fluxes in plumes from point sources in a turbulent boundary layer, *Journal of Fluid Mechanics* 117, pp. 1-26.

9. Grant A.L.M., 1986, Observations of boundary layer structure made during the 1981 KONTUR experiment, *Quarterly Journal of the Royal Meteorological Society* 112, pp. 825-841.

10. Henn D.S., Sykes R.I., 1992, Large-eddy simulation of dispersion in the convective boundary layer, *Atmospheric Environment* 26A**(17)**, pp. 3145-3159.

11. Kirkil G., Mirocha J., Bou-Zeid E., Chow F.K., Kosović B., 2012, Implementation and evaluation of subfilter-scale stress models for large-eddy simulation using WRF, *Monthly Weather Review* 140, pp. 266-284.

12. Moeng C-H., Sullivan P.P., 1994, A comparison of shear- and buoyancy-driven planetary boundary layer flows, *Journal of the Atmospheric Sciences* 51**(7)**, pp. 999-1022.

13. Moeng C-H., Dudhia J., Klemp J., Sullivan P., 2007, Examining two-way grid nesting for large eddy simulation of the PBL using the WRF model, *Monthly Weather Review* 135, pp. 2295-2311.

14. Nieuwstadt F.T.M., 1992, A large-eddy simulation of a line source in a convective atmospheric boundary layer – I. dispersion characteristics, *Atmospheric Environment* 26A**(3)**, pp. 485-495.

15. Piomelli U., Balaras E., 2002, Wall-layer models for large-eddy simulations, *Annual Review of Fluid Mechanics* 34, pp. 349-374.

16. Shaughnessy E.J., Morton J.B., 1977, Laser light-scattering measurements of particle concentration in a turbulent jet, *Journal of Fluid Mechanics* 80**(1)**, pp. 129-148.

17. Skamarock W.C., Klemp J.B., 2008, A time-split nonhydrostatic atmospheric model for weather research and forecasting applications, *Journal of Computational Physics* 227**(7)**, pp. 3465-3485.

18. Sloop C., Novakovskaia E., Continuous GHG monitoring at local to statewide scales, 4th NACP All-Investigators Meeting, Albuquerque, New Mexico.

19. Venkatram A., Wyngaard J.C. (Eds), 1988, Lectures on air pollution modeling, American Meteorological Society, Boston, 390 pgs.

20. Weil J.C., Synder W., Lawson Jr. R.E., Shipman M.S., 2002, Experiments on buoyant plume dispersion in a laboratory convection tank, *Boundary Layer Meteorology* 102, pp. 367-414.

21. Weil J.C., Sullivan P.P., Patton E.G., Moeng C-H., 2012, Statistical variability of dispersion in the convective boundary layer: ensembles of simulations and observations, *Boundary-Layer Meteorology* 145, pp. 185-210.

22. Welp L.R., Keeling R.F., Weiss R.F., Paplawsky W., Heckman S., 2012, Design and performance of a Nafion dryer for continuous operation at CO2 and CH4 air monitoring sites, *Atmospheric Measurement Techniques Discussions* 5, pp. 5449-5468.

23. Willis G.E., Deardorff J.W., 1976, A laboratory model of diffusion into the convective planetary boundary layer, *Quarterly Journal of the Royal Meteorological Society* 102**(432)**, pp. 427-445.

24. Willis G.E., Deardorff J.W., 1981, A laboratory study of dispersion from a source in the middle of the convectively mixed layer, *Atmospheric Environment* 15**(2)**, pp. 109-117.

25. Yee E., Chan R., 1997, A simple model for the probability density function of concentration fluctuations in atmospheric plumes, *Atmospheric Environment* 31**(7)**, pp. 991-1002.